

Topological Mott Insulators

S. Raghu¹, Xiao-Liang Qi¹, C. Honerkamp², and Shou-Cheng Zhang¹

¹*Department of Physics, McCullough Building, Stanford University, Stanford, CA 94305-4045 and*

²*Theoretical Physics, Universität Würzburg, D-97074 Würzburg, Germany*

(Dated: November 26, 2024)

We consider extended Hubbard models with repulsive interactions on a Honeycomb lattice and the transitions from the semi-metal phase at half-filling to Mott insulating phases. In particular, due to the frustrating nature of the second-neighbor repulsive interactions, topological Mott phases displaying the quantum Hall and the quantum spin Hall effects are found for spinless and spinful fermion models, respectively. We present the mean-field phase diagram and consider the effects of fluctuations within the random phase approximation (RPA). Functional renormalization group analysis also show that these states can be favored over the topologically trivial Mott insulating states.

PACS numbers: 71.10.-w, 71.10.Fd, 71.27.+a, 71.30.+h, 73.22.Gk, 73.43.-f

Introduction - Partly motivated by the discovery of the high T_c superconductivity, Mott insulators have attracted great attention in recent years. Defined in a general sense, interactions drive a quantum phase transition from a metallic ground state to an insulating ground state in these systems. Most Mott insulators found in nature also have conventional order parameters, describing, for example, the charge-density-wave (CDW) or the spin-density-wave (SDW) orders. However, Mott insulators with exotic ground states, such as the current carrying ground states have also been proposed theoretically [1, 2, 3, 4]. In parallel with the study of strongly correlated systems, there has recently been a growing interest in realizing topologically non-trivial states of matter in band insulators. In the quantum anomalous Hall (QAH) insulators[5, 6], the ground state breaks time reversal symmetry but does not break the lattice translational symmetry. The ground state has a bulk insulating gap, but has chiral edge states. In the quantum spin Hall (QSH) insulators[7, 8, 9], the ground state does not break time reversal symmetry, has a bulk insulating gap, but has helical edge states, where electrons with the opposite spins counter-propagate. The QSH state has recently been observed experimentally in $HgTe$ quantum wells[9, 10].

Given the tremendous interest in finding Mott insulators with exotic ground states, and the recent discovery of the topologically non-trivial band insulators, it is natural to ask whether one can find examples of topological Mott insulators, which we define as states with bulk insulating gaps driven by the interaction, and inside which lie topologically protected edge states. Furthermore, electronic states in the Mott insulator phases are characterized by topological invariants, namely, the $U(1)$ Chern number[11] in the case of the QAH state, and the Z_2 invariant[12] in the case of the QSH state. In this letter, we report on the first example of such a case by systematically studying Hubbard models with repulsive interactions on a two dimensional honeycomb lattice. In partic-

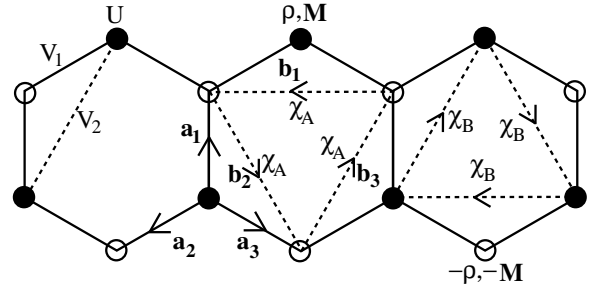


FIG. 1: Interactions considered in our model Hamiltonian (left-most hexagon), Eq. 1. Various order parameters are shown for the A-sublattice (open circles) in the middle hexagon and for the B-sublattice (filled circles) in the right-most hexagon. The CDW order parameter ρ is a real scalar, SDW order parameter \mathbf{M} a real vector and the QAH/QSH order parameters χ_A, χ_B are complex 4-vectors. In the case of spinless fermions, χ_A, χ_B are complex scalars. χ_A, χ_B are both defined on the directed second neighbor links defined by b_i .

ular, we demonstrate how, due to the frustrated nature of second-neighbor repulsion on this lattice, topological Mott phases displaying the QAH and the QSH effects are generated dynamically. We present the mean-field phase diagram, proceed to consider effects beyond mean-field theory via a functional renormalization group (fRG) treatment, and consider the effects arising from fluctuations. The two dimensional graphene sheet, which was recently realized experimentally [13, 14], contains the basic degrees of freedom of our model. However, presently we do not know how to tune the interaction experimentally so that our proposed state can be realized.

Spinless Fermions and the QAH state - The model Hamiltonian for spinless fermions with nearest-neighbor

and next-nearest neighbor interactions is written as

$$H = - \sum_{\langle ij \rangle} t \left(c_i^\dagger c_j + h.c. \right) + V_1 \sum_{\langle\langle i,j \rangle\rangle} (n_i - 1)(n_j - 1) + V_2 \sum_{\langle\langle i,j \rangle\rangle} (n_i - 1)(n_j - 1) - \mu \left(\sum_i n_i - N \right) \quad (1)$$

where V_1 and V_2 are nearest-neighbor and next-nearest-neighbor interaction strengths, respectively. Since the honeycomb lattice is bipartite, consisting of two triangular sublattices (referred to here as A and B), nearest-neighbor repulsion will favor a charge density wave (CDW) phase with an order parameter $\rho = \frac{1}{2} \left(\langle c_{iA}^\dagger c_{iA} \rangle - \langle c_{iB}^\dagger c_{iB} \rangle \right)$ that is consistent with overall charge conservation and describes a phase with a broken discrete (inversion) symmetry. However, since the second neighbor interactions within a sublattice are frustrated, CDW order will be suppressed; instead we consider the possibility of orbital ordering by defining the following order parameter for i, j next nearest neighbors: $\chi_{ij} = \chi_{ji}^* = \langle c_i^\dagger c_j \rangle$. Let $\mathbf{a}_1, \mathbf{a}_2, \mathbf{a}_3$ be the nearest-neighbor displacements from a B-site to an A-site such that $\mathbf{z} \cdot \mathbf{a}_1 \times \mathbf{a}_2$ is positive. We also define the displacements $\mathbf{b}_1 = \mathbf{a}_2 - \mathbf{a}_3$, $\mathbf{b}_2 = \mathbf{a}_3 - \mathbf{a}_1$, etc, which connect two neighboring sites on the same sublattice (Fig. 1). A translational and rotational invariant ansatz of χ_{ij} is chosen as

$$\chi_{i, i+\mathbf{b}_s} = \begin{cases} \chi_A = |\chi| e^{i\phi_A}, & i \in A \\ \chi_B = |\chi| e^{i\phi_B}, & i \in B \end{cases} \quad (2)$$

which are *complex* scalars that live along the directed second neighbor links.

Owing to translational symmetry, the mean-field free energy at $T = 0$ is readily obtained:

$$F(\rho, \chi, \bar{\phi}, \phi) = - \sum_{\mathbf{k}} \sqrt{|t(\mathbf{k})|^2 + (V_1 \rho + 2V_2 |\chi| S_{\mathbf{k}+\bar{\phi}} S_\phi)^2} + 3L^2 (V_1 \rho^2 + 2V_2 |\chi|^2) \quad (3)$$

We have defined the following quantities: $t(\mathbf{k}) = \sum_{n=1}^3 \exp(i\mathbf{k} \cdot \mathbf{a}_n)$, $\bar{\phi} = (\phi_A + \phi_B)/2$, $\phi = (\phi_A - \phi_B)/2$, $S_{\mathbf{k}+\bar{\phi}} = \sum_{n=1}^3 \sin(\mathbf{k} \cdot \mathbf{b}_n + \bar{\phi})$, $S_\phi = \sin \phi$. Thus, the next-neighbor hopping amplitudes are purely real only when both $\phi = 0$ and $\bar{\phi} = 0$.

When both ρ and $\chi = 0$, and at half-filling, the system remains a semi-metal consisting of two Fermi points \mathbf{K}_\pm which obey $\mathbf{K}_\pm \cdot \mathbf{b}_i = \pm 2\pi/3$ and the density of states vanishes linearly; the dispersion in the vicinity of these so called Dirac points is governed by a 2D massless Dirac Hamiltonian in \mathbf{k} -space. The CDW phase corresponds to an ordinary insulator with a gap at the Fermi energy. As for the order parameter χ , which describes the second-neighbor hopping, its *phase* relative to the nearest neighbor hopping amplitude plays an important

role in determining its properties: while a non-zero $Re(\chi)$ merely shifts the energy of the Dirac points, a non-zero imaginary part $Im(\chi)$ *opens a gap* at the Fermi points. Thus, when the system remains at half-filling, it is more favorable to develop purely imaginary next-neighbor hopping amplitudes; such a configuration corresponds to a phase with *spontaneously broken time-reversal symmetry*.

To see whether such a phase can be favored, we minimize the free-energy and arrive at the following self-consistent equations:

$$\rho = \frac{1}{2L^2} \sum_{\mathbf{k}} \frac{V_1 \rho + 2V_2 \chi S_{\mathbf{k}+\bar{\phi}} S_\phi}{\sqrt{|t(\mathbf{k})|^2 + (V_1 \rho + 2V_2 \chi S_{\mathbf{k}+\bar{\phi}} S_\phi)^2}} \quad (4)$$

$$\chi = \frac{S_\phi}{6L^2} \sum_{\mathbf{k}} \frac{S_{\mathbf{k}+\bar{\phi}} (V_1 \rho + 2V_2 \chi S_{\mathbf{k}+\bar{\phi}} S_\phi)}{\sqrt{|t(\mathbf{k})|^2 + (V_1 \rho + 2V_2 \chi S_{\mathbf{k}+\bar{\phi}} S_\phi)^2}} \quad (5)$$

When $\chi = 0$, it is easy to see from the first equation above that CDW order develops continuously at a critical value V_{1c} given by

$$\frac{1}{V_{1c}} = \frac{1}{2L^2} \sum_{\mathbf{k}} \frac{1}{|t(\mathbf{k})|}, \quad (6)$$

Due to the vanishing density of states (DOS) near the Fermi points, there is no instability towards CDW formation with infinitesimal interactions. Interestingly, the self-consistent equation for χ shows that a non-trivial self-consistent solution can only occur when $\phi \neq 0$; a detailed investigation of these equations [15] show that when $V_1 = 0$, beyond a critical value of $V_{2c} > 0$, which satisfies

$$\frac{1}{V_{2c}} = \frac{1}{3L^2} \sum_{\mathbf{k}} \frac{S_{\mathbf{k}+\bar{\phi}}^2}{|t(\mathbf{k})|}, \quad (7)$$

a phase in which $|\chi| > 0$, $\bar{\phi} = 0$, and $\phi = \pm\pi/2$ is favored. Such a phase is also stable at finite V_1 and is thus does not require fine-tuning (see Fig. 2). In this phase, the system acquires purely imaginary second-neighbor hoppings with a chirality which is determined by the sign of ϕ . There is a discrete symmetry breaking corresponding to choosing $\phi = \pm\pi/2$, each of which breaks time-reversal symmetry. The band insulator version of the CDW state was considered in Ref. [16], while the QH state on a honeycomb lattice was considered in Ref. [5]. As discussed in Ref. [5] the QAH phase is a topological phase in which the filled states form a band which has a non-zero topological Chern number [11] and is an integer quantum Hall effect phase that is realized *without* Landau levels. Similar states can be constructed from magnetic semiconductors[6]. We shall generally refer to QH states without Landau levels, and with full lattice translation symmetry as the *Quantum Anomalous Hall* (QAH) states. In our case, the topologically non-trivial

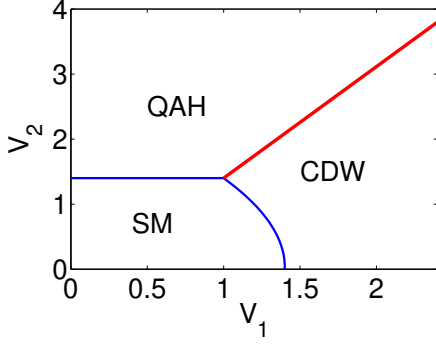


FIG. 2: Phase diagram for spinless fermions ($t = 1$). The semi-metallic (SM) state that occurs at weak-coupling is separated from the CDW and the topological QAH states via a continuous transition (blue curve). The line separating the QAH and CDW marks a first-order transition (shown in red), which terminates at a bi-critical point.

gap for the QAH state arises from many-body interactions rather than single particle physics, and we shall refer to such states as topological Mott insulators.

We have obtained the complete phase diagram in the $V_1 - V_2$ plane; within mean-field theory, there is a continuous transition from the semi-metal to either the CDW or the QAH phase and there is also a first-order transition from the CDW to the QAH phase. By integrating out the fermionic fields, it is possible to construct a Landau-Ginzburg (LG) theory expansion near the nodal region where the order parameters are vanishingly small. Due to the linear dispersion of the Fermi points, the LG free-energy contains anomalous terms of the form $|\rho|^3$ and $|Im(\chi)|^3$ arising from linear dispersion in the vicinity of the Fermi points [15]. The significance of such terms is that even within mean-field theory, the CDW order parameter, for instance, grows as $(V_1 - V_{1c})$ rather than the usual $(V_1 - V_{1c})^{1/2}$ [17]. Furthermore, the Landau-Ginzburg theory describing the competition between the CDW and QAH phases confirms the existence of the first order line between these two phases that terminates in the bicritical point leading into the semimetal phase [15].

Spinful fermions and the QSH state - Next, we take into account the spin degrees of freedom and include an onsite Hubbard repulsion in our model Hamiltonian ($\mu = 0$):

$$H = - \sum_{\langle ij \rangle \sigma} t \left(c_{i\sigma}^\dagger c_{j\sigma} + h.c. \right) + U \sum_i n_{i\uparrow} n_{i\downarrow} + V_1 \sum_{\langle i,j \rangle} (n_i - 1)(n_j - 1) + V_2 \sum_{\langle\langle i,j \rangle\rangle} (n_i - 1)(n_j - 1) \quad (8)$$

where $n_i = n_{i\uparrow} + n_{i\downarrow}$. Since the Honeycomb lattice is bipartite, onsite repulsion gives rise to a spin density wave phase (SDW); a standard decomposition of the Hubbard term introduces the order parameter \mathbf{M} describing an

antiferromagnetic SDW: $\mathbf{M} = \frac{1}{2} (\langle \mathbf{S}_{iA} \rangle - \langle \mathbf{S}_{iB} \rangle)$. As in the spinless case, nearest-neighbor repulsion favors a CDW. However, there are several possible phases due to second-neighbor repulsion. Again, since the second-neighbor repulsion is frustrated, we are again led to the possibility of a topological phase similar to the QAH. However, the spin degrees of freedom introduce two possibilities (translation invariance along with spin conservation eliminate other possibilities): 1) *two copies* of QAH states - i.e. the chirality of the second-neighbor hopping is the *same* for each spin projection, 2) the QSH state, where the chiralities are *opposite* for each spin projection. The latter possibility breaks a *continuous* global $SU(2)$ symmetry associated with choosing the spin projection axis; however, *time-reversal symmetry is preserved*. The QSH state on the honeycomb lattice was considered in Ref. [7], where the insulating gap arises from the microscopic spin-orbit coupling. It was shown latter that the magnitude of the spin-orbit gap is negligibly small in graphene [18, 19]. In our case, the insulating gap is generated dynamically from the many-body interaction. In this sense, our effect can be viewed as an example of dynamic generation of spin-orbit interaction[20]. Introducing the Hubbard-Strataovich fields (sum over repeated indices implied) $\chi_{ij}^\mu = c_{i\alpha}^\dagger \sigma_{\alpha\beta}^\mu c_{j\beta}$, $\mu = 0 \dots 3$, where $\sigma^\mu = (1, \boldsymbol{\sigma})$, the next-neighbor interactions can be recast using the identity $(n_i - 1)(n_j - 1) = 1 - \frac{1}{2} (\chi_{ij}^\mu)^\dagger \chi_{ij}^\mu$. Physically, if $\langle \chi^0 \rangle \neq 0$, then we are in the QAH phase. If, on the other hand, one of the vector components $\langle \chi^i \rangle \neq 0$, then we are in the QSH phase. A translationally invariant decomposition of the next-neighbor interactions via $\langle \chi_{i,i+\mathbf{b}_s}^\mu \rangle = \chi^\mu e^{i\phi_A^\mu}$, $i \in A$ (and similarly for the other sublattice) gives rise to a 4×4 Hamiltonian is readily diagonalized in a tensor product basis $\boldsymbol{\sigma} \otimes \boldsymbol{\tau}$, where $\boldsymbol{\sigma}$ and $\boldsymbol{\tau}$ are Pauli matrices in spin and sublattice space, respectively. This way, each phase corresponds to a particular non-zero expectation value of a fermion bilinear $\sum_{\vec{k}} \Psi_{\vec{k}}^\dagger \hat{d}(\vec{k}) \Psi_{\vec{k}}$, where $\hat{d}(\vec{k}) \propto \tau^3$ for the CDW and QAH, $\hat{d}(\vec{k}) \propto \sigma^3 \tau^3$ for SDW and QSH. A detailed study of the free-energy at $T = 0$ and its saddle point solutions [15] produces the phase diagram shown in Fig. 3. In addition to the ordinary CDW and SDW insulating phases, there is a phase for $V_2 > V_{2c} \approx 1.2t$ in which the 4-vector is purely imaginary (as in the spinless case), collinear, and staggered from one sublattice to the next: $\langle \chi_{ii+\mathbf{b}_n,A}^\mu \rangle = -\langle \chi_{ii+\mathbf{b}_n,B}^\mu \rangle$, and both QAH and QSH are equally favorable ground states, having identical free energies within mean-field theory. Additionally, there is never a coexistence of both QAH and QSH phases; indeed, a Landau-Ginzburg treatment in this region explicitly shows the absence $SO(4)$ symmetry of the vector χ^μ . This occurs due to the difference of the manner in which χ^0 and $\vec{\chi}$ are coupled to the fermionic fields - which favors either a phase with broken Z_2 symmetry (QAH) or with broken $SU(2)$ symmetry, but never both simultaneously

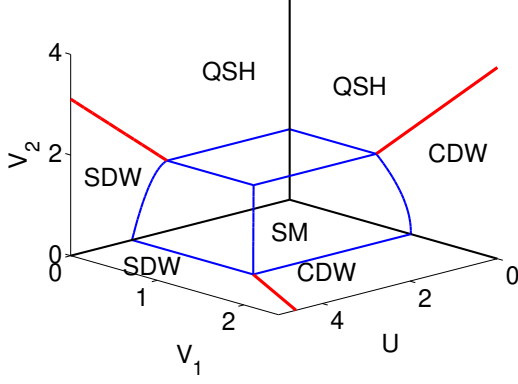


FIG. 3: Complete mean-field phase diagram for the spinful model. The transitions from the semimetal (SM) to the insulating phases are continuous, whereas transitions between any two insulating phases (red lines) are first-order.

[15].

Quantum fluctuations, however, lift the mean-field degeneracy between the QAH and QSH phases. To quadratic order in quantum fluctuations (RPA) about the QSH phase, we obtain an effective action $S_{eff} = \sum_{\vec{k}} \delta\chi^\mu(\vec{k}, \Omega) K_{\mu\nu}(\vec{k}, \Omega) \delta\chi^\nu(-\vec{k}, -\Omega)$ which shows the presence of six modes (2 longitudinal and 4 transverse modes), and 2 of the transverse modes correspond to degenerate Goldstone modes whose velocity is proportionality to the Fermi velocity $v \approx v_f = 3t/2|a|$. Thus, the zero-point motion associated with these gapless modes, lowers the free energy of the QSH state relative to the QAH state.

Renormalization Group Analysis - Mean field theory generally starts with a given, in a sense, biased Ansatz, and investigate the self-consistency of the mean field solution. Therefore, it is important to investigate the topological Mott states with a method without any a priori bias. Next we go beyond mean-field theory and RPA using the temperature(T)-flow functional renormalization group (fRG)[21][22]. In this scheme, we discretize the \vec{k} -dependence of the interaction [23] and consider all possible scattering processes between a set of initial and final momenta that occur between points on rings around the Dirac points (inset of Fig. 4). Starting with $T_0 \sim 2t$, the temperature T is lowered, and a flowing (renormalized) interaction V_T is obtained by the coupled summation of the T -derivatives of *all* one-loop channels. Due to this, the method is unbiased and goes beyond the mean-field-level. Applying the scheme to the Hamiltonian, Eq. 8, we search for *flows to strong coupling*, where for a low temperature T_c certain components of V_T become large. Then the approximations break down, and the flow is stopped. Information on the low- T state is obtained from analyzing which coupling functions grow most strongly and from susceptibilities for static external

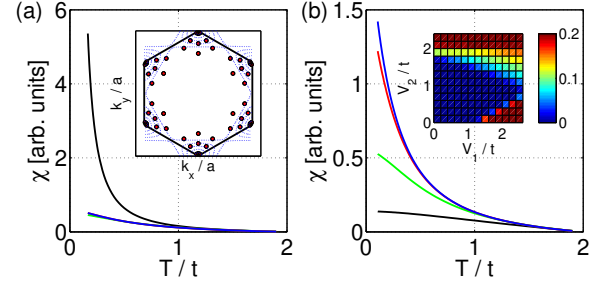


FIG. 4: *a)* Data for $U=0$, $V_1=1.4t$, $V_2=0$. Susceptibilities of each phase vs. T are shown: CDW (black); SDW (green); QAH (red) and QSH (blue). *b)* Same for $U=0$, $V_1=0$, $V_2=1.8t$ (QSH instability). The QSH phase has a larger susceptibility than QAH. *Inset:* fRG phase diagram at $U=0$, indicating SM (blue) and insulating (red) regions (CDW dominates at large V_1 , QSH at large V_2 .) The colorbar correspond to T_c below which the insulating phases develop in fRG.

fields coupling to the various order parameters. In this scheme, a tendency towards ordering at a finite vector \mathbf{Q} can be detected as a growth of the associated vertex V_T . However, we have found that largest couplings occur at $\mathbf{Q} = 0$, which strongly supports the mean-field results presented above.

For onsite and nearest-neighbor repulsions $U > U_c \approx 3.8t$ and $V_1 > V_{1c} \approx 1.2t$, the flow to strong coupling is either an SDW instability for dominant U or a CDW instability for dominant V_1 , in good agreement with a $1/N$ -study[24] and Quantum-Monte-Carlo[17]. For more details, see Ref. [25]. If we include a sufficiently strong second-nearest-neighbor repulsion $V_2 > 1.6t$, the flows change qualitatively; there is a leading growth of the QSH susceptibility. In Fig. 4 a) and b) we compare the T -flows of various susceptibilities for $V_1 > V_2$ and for $V_2 > V_1$. For the latter case, the QSH susceptibility grows most strongly toward low T , followed by the QAH susceptibility, which is consistent with the RPA treatment of the Goldstone modes in the QSH. The QSH phase remains stable even when a moderate onsite interaction of $U = t$ or $U = 2t$ is introduced. Hence the global structure of the mean-field phase diagram is confirmed by the fRG results. Note however that the slope of the lines of critical V_1 versus V_2 differs. We interpret this a competition effect captured by the fRG, where V_2 decreases the CDW tendencies induced by V_1 .

Discussion - We have shown that topological phases displaying the QAH and QSH effects can be generated from strong interactions - thus, we refer to these phases as *topological Mott insulators*. Both phases have associated with them conventional order parameters which develop continuously at the quantum critical phase transition from the semi-metallic state. However, these states are also described by topological quantum numbers which jump discontinuously at the transition. Although the interaction strengths needed to produce these phases are

strong, we expect that our mean-field, RPA and fRG treatment to provide strong evidence for the existence of a topological Mott insulator: the Stoner criterion, which states that perturbation theory breaks down when interaction strengths are comparable to the inverse of the effective DOS, suggests that perturbation theory is more robust in our system due to the vanishing of the DOS at the Fermi points. An open issue remains to find other possible realizations of the phases described here. Furthermore, the nature of the low energy effective coupling of the gapless bulk Goldstone modes with the gapless *edge* degrees of freedom, and the possibility of fractionalized excitations in these phases are interesting open issues that we leave for future work.

ACKNOWLEDGMENTS

We are grateful to D. P. Arovas and S. A. Kivelson for insightful discussions. This work is supported by the NSF under grant numbers DMR-0342832, the US Department of Energy, Office of Basic Energy Sciences under contract DE-AC03-76SF00515, BaCaTec (C.H.), and the Stanford Institute for Theoretical Physics (S.R.).

-
- [1] I. Affleck and J. B. Marston, Phys. Rev. B **37**, 3774 (1988).
 - [2] X.-G. Wen and P. A. Lee, Phys. Rev. Lett. **76**, 503 (1996).
 - [3] C. M. Varma, Phys. Rev. Lett. **83**, 3538 (1999).
 - [4] S. Chakravarty, R. B. Laughlin, D. K. Morr, and C. Nayak, Phys. Rev. B p. 094503 (2001).
 - [5] F. D. M. Haldane, Phys. Rev. Lett. **61**, 2015 (1988).
 - [6] X. L. Qi, Y. S. Wu, and S. C. Zhang, Phys. Rev. B **74**, 085308 (2006).
 - [7] C. L. Kane and E. J. Mele, Phys. Rev. Lett. **95**, 226801 (2005).
 - [8] B.A. Bernevig and S.C. Zhang, Phys. Rev. Lett. **96**, 106802 (2006).
 - [9] B. A. Bernevig, T. L. Hughes, and S.C. Zhang, Science **314**, 1757 (2006).
 - [10] M. Konig, S. Wiedmann, C. Brune, A. Roth, H. Buhmann, L. Molenkamp, X.-L. Qi, and S.-C. Zhang, *Science*, to be published.
 - [11] D. J. Thouless, M. Kohmoto, M. P. Nightingale, and M. den Nijs, Phys. Rev. Lett. **49**, 405 (1982).
 - [12] C. L. Kane and E. J. Mele, Phys. Rev. Lett. **95**, 146802 (2005).
 - [13] K. S. Novoselov, A. K. Geim, S. V. Morozov, D. Jiang, M. I. Katsnelson, I. V. Grigorieva, S. V. Dubonos, and A. A. Firsov, Nature **438**, 197 (2005).
 - [14] Y. Zhang, Y.-W. Tan, H. L. Stormer, and P. Kim, Nature **438**, 201 (2005).
 - [15] S. Raghu, X.-L. Qi, C. Honerkamp, and S.-C. Zhang, In preparation.
 - [16] G. Semenoff, Phys. Rev. Lett. **53**, 2449 (1984).
 - [17] S. Sorella and E. Tosatti, Europhysics Letters **49**, 699 (1992).
 - [18] H. Min, J. E. Hill, N. A. Sinitsyn, B. R. Sahu, L. Kleinman, and A. H. MacDonald, Phys. Rev. B **74**, 165310 (2006).
 - [19] Y. Yao, F. Ye, X.-L. Qi, S.-C. Zhang, and Z. Fang, Phys. Rev. B **75**, 041401(R) (2007).
 - [20] C. Wu and S.-C. Zhang, Phys. Rev. Lett. **93**, 036403 (2004).
 - [21] C. Honerkamp and M. Salmhofer, Phys. Rev. B **64**, 184516 (2001).
 - [22] C. Honerkamp and M. Salmhofer, Phys. Rev. Lett. **87**, 187004 (2001).
 - [23] D. Zanchi and H. J. Schulz, Phys. Rev. B **61**, 13609 (2000).
 - [24] I. F. Herbut, Phys. Rev. Lett. **97**, 146401 (2006).
 - [25] C. Honerkamp, In preparation.